Grating Assisted Coupling of Light Between Semiconductor and Glass Waveguides *

Jerome K. Butler, Nai-Hsiang Sun and Gary A. Evans
Southern Methodist University
Dallas, TX 75275
Lily Pang and Phil Congdon
Texas Instruments, Inc.
Dallas, TX 75243

February 28, 2003

Abstract

Floquet-Bloch theory is used to calculate the electromagnetic fields in a leaky-mode grating-assisted directional coupler (LM-GADC) fabricated with semiconductor and glass materials. One waveguide is made from semiconductor materials (refractive index ≈ 3.2) while the second is made from glass (refractive index ≈ 1.45). The coupling of light between the two waveguides is assisted by a grating fabricated at the interface of the glass and semiconductor materials. Unlike typical GADC structures where power is exchanged between two waveguides using bound modes, this semiconductor/glass combination couples power between two waveguides using a bound mode (confined to the semiconductor) and a leaky mode (associated with the glass). The characteristics of the LM-GADC are discussed. Such LM-GADC couplers are expected to have numerous applications in areas such as laser-fiber coupling, photonic integrated circuits, and on-chip optical clock distribution. Analyses indicate that simple LM-GADCs can couple over 40 % of the optical power from one waveguide to another in distances less than 1.25 mm.

*This work was supported by DARPA under Contract DAAL01-95-C-3524

I. Introduction

The ability to couple diode laser outputs monolithically and efficiently to a low loss co-integrated glass optical waveguide will enable applications such as large scale photonic integrated circuits, on chip optical clock distributions for high speed microprocessors, and compact wavelength division multiplexing laser sources.

In this paper, we present a new architecture of an integrated grating-assisted directional coupler (GADC) which is made of a III-V waveguide ($n_{\text{eff}} \approx 3.2$) and a phosphorus-doped silica glass (PSG) waveguide ($n_{\text{eff}} \approx 1.45$). The use of glass waveguides offers the combination of very low loss ($<$0.01 dB/cm), silicon process compatibility, and simple, low cost fabrication processes. In addition, the PSG waveguide can have mode fields that are nearly identical in shape to the fields of a single-mode fiber. The near perfect match of properly designed PSG waveguide optical fields with those of an optical fiber produces $>$95 % butt coupling between the PSG waveguide and a single mode optical fiber without external optics.

A GADC consisting of two non-synchronous waveguides and a separate grating region is in reality a single, composite waveguide. However, for clarity, we will refer to two sub-waveguides called "sub-waveguide S (semiconductor)" and "sub-waveguide G (glass)". In applications such as the one discussed in this paper the geometry of the two waveguides (waveguide dimensions as well as their corresponding refractive indices) are greatly different. Assuming the two waveguides S and G are uncoupled and that each supports only a single mode, the modes of the two individual guides would have large differences in their effective indices. To strongly couple the two waveguides, a grating is designed to phase-match the longitudinal propagation constants of the individual waveguides. In GADCs consisting of two guides with similar refractive indices but with different geometrical shapes, the effective indices of the individual modes are similar. In the latter case, the grating wavenumber, used to phase-match the longitudinal propagation constants of the individual modes is rather small. Table I shows refractive indices and layer thicknesses of such an extensively studied GADC structure [1]. Although the two coupled waveguides are not identical, each supports a bound mode and each is composed of "similar" materials.

Figure 1 shows a cross section of a leaky-mode grating-assisted directional coupler (LM-GADC), which consists of a laser waveguide integrated with a PSG waveguide. The codirectional grating coupler, in the central region of the figure, has a grating layer of length L_g. The rectangular-tooth grating layer is composed of semiconductor material in one region and glass in the other. Outside the grating region ($z < 0$ and $z > L_g$), the two sub-waveguides have negligible interaction, i.e., no significant power can be coupled from the semiconductor sub-waveguide to the glass sub-waveguide and vice versa. In this study, the LM-GADC is excited with a laser mode, where the optical field is predominantly confined to the semiconductor waveguide, at the LM-GADC input, $z = 0$. The coupling efficiency is computed by calculating the percentage of power at the input that is coupled to the glass waveguide at the output, $z = L_g$. In the region $z > L_g$, there will be no interaction between the two sub-waveguides.

The analysis of the coupling between the glass and semiconductor layers is for a slab structure. (The geometry has infinite extensions along the lateral y direction.) Accordingly,

the results obtained are reasonably accurate for a structure whose transverse mode width (x-direction) is small compared to the lateral mode width (y-direction).

The index profile of the semiconductor-glass LM-GADC is shown in Fig. 2. Unlike typical GADCs, where the power exchange between the two sub-waveguides occurs *via* bound modes, the semiconductor-glass LM-GADC exchanges power between sub-waveguides using a bound mode of the semiconductor sub-waveguide and a (fundamental) leaky mode of the glass sub-waveguide. In Fig. 2 the index of refraction of the core in the glass region is much smaller than the index of refraction of the semiconductor substrate. This high index mismatch causes the modes of the glass waveguide to leak energy to the semiconductor substrate. As a result, mode propagation in the glass waveguide attenuates due to power loss to the semiconductor substrate.

The concept of the grating coupler causing the two lowest-order modes of the composite waveguide to have similar power distributions in each sub-waveguide was developed in [2] for typical GADCs. This same concept and the resulting physical processes for power exchange between the two sub-waveguides applies directly to LM-GADCs. However in the latter device, the losses of each sub-waveguide can be large and unequal. As a result of these large and unequal losses, the maximum power transfer between sub-waveguides occurs before the power in the other sub-waveguide is a minimum.

The most common, simple, and intuitive theoretical analyses of the GADC are based on coupled-mode theory (CMT) which finds the coupling length, the coupled power distribution, and the resonant grating period [1],[3] –[14]. Also, a transfer matrix method (TMM) approach using the mode-matching technique has been introduced to examine the power coupling and radiation loss of the GADC structure [15]. To date, CMT or TMM approaches have not been applied to GADC structures with interacting leaky modes or to structures with layers that have material losses.

Rather than add corrections to the CMT or TMM approaches, we use the Floquet-Bloch theory [16]–[19] to analyze the LM-GADC problem because it accounts for radiation losses from leaky modes as well as material losses in the various layers in a straightforward manner. In general, the Floquet-Bloch analysis calculates radiation losses of the LM-GADC from fundamental principles [2].

In Section II, a brief introduction of the Floquet-Bloch theory [17] is presented. An example of the typical GADC is discussed in Section III. Then, we analyze the LM-GADC structure shown in Figs. 1 and 2. The complete field distributions and dispersion and attenuation characteristics are discussed in Section IV. In Section V, the power coupling mechanism of the semiconductor-glass LM-GADC is discussed.

II. Problem Formulation

Consider a dielectric waveguide with arbitrary layers including a periodic grating layer. The dielectric superstrate and substrate regions are assumed to be half spaces. The dielectric materials in each layer (except the grating layer) are isotropic and homogeneous. A wave with time variation of the form $\exp(j\omega t)$ is assumed to propagate in the z direction (see Fig. 1), as $\exp(-\gamma z)$. The complex longitudinal propagation constant is $\gamma = \alpha + j\beta$. For the sake of simplicity assume the field is invariant with respect to y.

Characteristic Modes

For the GADC and LM-GADC structures, the field expressions which are written in Floquet-Bloch form must satisfy the boundary conditions at each interface. Assuming transverse electric (TE) polarization, the y-component of the electric field in the *i*-th layer, $E_y^{(i)}$, can be written as

$$\begin{aligned} E_y^{(i)}(x,y) &= f^{(i)}(x,z)\, e^{-\gamma z} \\ &= e^{-(\alpha+j\beta)z} \sum_{n=-\infty}^{\infty} f_n^{(i)}(x) e^{-jnKz} = \sum_{n=-\infty}^{\infty} f_n^{(i)}(x) e^{-jk_{zn}z}, \end{aligned} \tag{1}$$

where $K = 2\pi/\Lambda$ is the grating wavenumber, Λ is the grating period, n is the space harmonic order, i indicates the i-th layer, and $f_n^{(i)}$ is the amplitude of the nth space harmonic. The function $f^{(i)}$ is periodic and satisfies $f^{(i)}(x,z) = f^{(i)}(x,z+\Lambda)$. The term k_{zn} is the complex propagation constant of the nth spatial harmonic and can be written as

$$k_{zn} = (\beta + nK) - j\alpha = \beta_n - j\alpha, \tag{2}$$

where β_n, the real part of k_{zn}, is the longitudinal propagation constant of the n-th space harmonic, and α (> 0), the imaginary part of k_{zn}, is the attenuation constant due to leaky modes as well as material losses. Similarly, the magnetic field along the z direction in the ith layer, $H_z^{(i)}$ can be expressed as

$$H_z^{(i)} = \sum_{n=-\infty}^{\infty} h_n^{(i)}\, e^{-jk_{zn}z}, \tag{3}$$

where $h_n^{(i)}$ is the nth space harmonic component of the magnetic field in the ith layer. Outside the grating layer, the scalar Helmholtz equation can be written as

$$\frac{d^2 f_n^{(i)}(x)}{dx^2} + [k^2\varepsilon_i - k_{zn}^2]\, f_n^{(i)}(x) = 0, \tag{4}$$

where $k = 2\pi/\lambda$ is the free space wavenumber, ε_i is the relative dielectric constant of the ith layer, and the complex transverse wavenumber for the nth space harmonic in the ith layer is defined by $(k_{zn}^{(i)})^2 = \varepsilon_i k^2 - k_{zn}^2$.

The interesting features of Floquet-Bloch modes, including the generation of space harmonics results from the periodic grating layer. Because the refractive index in the grating layer is nonuniform and varies periodically along the propagation direction, the permittivity can be expressed as a Fourier series

$$\varepsilon(x,z) = \sum_n \varepsilon_n(x)\, e^{jnKz}. \tag{5}$$

The field solution for TE modes in the grating layer is obtained by solving the equivalent Maxwell's equations instead of (4):

$$\frac{d\vec{f}^{(g)}}{dx} = \mathbf{Q}(k_{z0}\cdot)\vec{h}^{(g)}(x), \tag{6}$$

and

$$\frac{d\vec{h}^{(g)}}{dx} = \mathbf{P}(k_{z0}\cdot)\,\vec{f}^{(g)}(x), \tag{7}$$

where g stands for the grating layer, and the variable k_{z0} is the complex propagation constant of the 0-th spatial harmonic. The vectors $\vec{f}^{(g)}(x)$ and $\vec{h}^{(g)}(x)$ are formed by the group of spatial harmonics $f_n^{(g)}(x)$ and $h_n^{(g)}(x)$, respectively, where $f_n^{(g)}(x)$ and $h_n^{(g)}(x)$ are defined by (1) and (3). For TE polarization, the square matrices $\mathbf{P}(k_{z0})$ and $\mathbf{Q}(k_{z0})$ have elements $P_{nm} = j\omega\varepsilon_0[(k_{zn}/k)^2\delta_{nm} - \varepsilon_{n-m}]$ and $Q_{nm} = j\omega\mu_0\delta_{nm}$, respectively, where δ_{nm} is the Kronecker delta.

The solutions of the Helmholtz equation (4) are given by the linear combination of $\exp(jk_{zn}^{(i)}x)$ and $\exp(-jk_{zn}^{(i)}x)$, while the equivalent Maxwell's equations (6) and (7) can be solved by the fourth-order Runge-Kutta method [20]. A resulting characteristic equation is obtained by appropriately matching the boundary conditions and simultaneously solving (6) and (7). Considering transverse electric polarization, the field components and their normal derivatives must be continuous at each interface. After appropriate substitution, we obtain a system of linear equations $\mathbf{D}(k_{z0}) \cdot \vec{f}(x_{k-1}) = 0$ with the unknown variable k_{z0}, where $\mathbf{D}$ is a square matrix, and $\vec{f}(x_{k-1})$ is the initial value of the field at the bottom of the grating layer. The system of linear equations has a nontrivial solution when[2]

$$\det[\mathbf{D}(k_{z0})] = 0. \tag{8}$$

After solving for the roots of (8) numerically[20], the Floquet amplitudes of all space harmonics for the field distribution in all layers can be evaluated.

Kinematic Properties

Many of the modal interaction features of grating-assisted couplers can be understood by analyzing the "$\omega - \beta$" plot shown in Fig. 3. (The lines in the figure do not represent the actual dispersion curves of the modes or the space harmonics.) In the present case we will consider two Floquet-Bloch modes of the LM-GADC, labeled mode A and mode B. When the modes do not interact, say at some position below resonance (small Λ values), mode A represents the mode of the semiconductor waveguide, while mode B represents the mode of the glass waveguide. Away from resonance the field distribution of the modes will be almost identical to the modes of the individual sub-waveguides in the absence of the other. Mode A has an effective index, n_A, that lies between 3.386 and 3.165, while mode B has an effective index, n_B, lying between 1.458 and 1.448. The lower bound on n_A is 3.165 and the lower bound for n_B is 1.448. In Fig. 3, the slope of the line representing mode A is 1/3.165 and the slope of the line representing mode B is 1/1.448. The actual dispersion curves will lie slightly below the two dark lines of the figure.

The space harmonics for the two modes intersect at an infinite number of positions, represented by the points $I_{i,j}$, where i represents the space harmonic of mode A and j represents the space harmonic of mode B. The two cone regions about the $k\Lambda$ axis are the superstrate fast-wave region (FWR) and substrate FWR. It should be noted that the

fundamental space harmonic for mode B lies in the FWR of the substrate. This means that for any grating period the glass mode will be leaky. At resonance, where the lines cross, there can be a number of leaky space harmonics. Figure 3 shows 4 such intersection points in the substrate FWR. The points to the right of the $k\Lambda$ axis represents leaky mode radiation in the forward direction of the substrate while the points to the left of the axis represents leaky mode radiation in the backward direction of the substrate. Assuming $1/n_A$ and $1/n_B$ are the slopes of the lines representing the two modes, the number of space harmonics that leak to the substrate is the integer value N = Int$[2n_A/(n_A - n_B)]$. The GADC of Table I has over 60 leaky space harmonics near resonance while the LM-GADC (Table II) has only 4 leaky space harmonics.

Since strong modal coupling occurs only in the vicinity of the intersection points of Fig. 3, the dispersion curves for the two modes will be shown only in the neighborhood of the $I_{0,1}$ intersection. The relative shapes of the dispersion curves in the neighborhood of $I_{i,j}$ are identical to the curve shapes around the $I_{0,1}$ intersection.

III. Grating-Assisted Directional Couplers

The conventional GADC problem, originally analyzed by Marcuse[1], can be solved using the Floquet-Block theory [2]. The vacuum wavelength is assumed to be 1.5 μm in Table I. Figure 4 represents the typical characteristics of two interacting Floquet-Bloch modes and shows the normalized real and imaginary parts of the propagation constants, for modes A and B as a function of the grating period for the structure of Table I. The two curves in Fig. 4(b) correspond to β_0^A and β_1^B where β_0^A indicates the real part of the propagation constant of the $n = 0$ space harmonic for mode A, and β_1^B is that of the $n = 1$ space harmonic for mode B.

When two modes are interacting at resonance, requirements for strong coupling include

1. phase-matching between one space harmonic of one mode with another space harmonic of the interacting mode, and

2. the intensity distributions of the two modes must be similar (as close as possible).

It can be seen from Fig. 4 that the first condition is met for a range of grating periods, Λ, which satisfy

$$\beta_1^B - \beta_0^A = \delta(\Lambda), \tag{9}$$

where the propagation constant of the first space harmonic satisfies

$$\beta_1^B = \beta_0^B + K, \tag{10}$$

so that Eq. (9) becomes

$$K = \delta(\Lambda) + \beta_0^A - \beta_0^B. \tag{11}$$

Equation (11) provides a relationship between the grating period $\Lambda = 2\pi/K$ and the longitudinal propagation constants of mode A and mode B and the "deviation wavenumber" δ (see Fig. 4).

Although Eq. (11) insures phase matching, it does not guarantee that a large fraction of power will be transferred between sub-waveguides. To insure significant power transfer the modes must have nearly identical power distributions (the second condition above). Modes A and B are closest to having identical intensity shapes when their longitudinal propagation constants differ by approximately K, the grating wavenumber. This occurs when δ is a minimum.

The normalized attenuation for the two modes for the structure of Table I is shown in Fig. 4. It should be noted that all space harmonics for each mode exhibit identical attenuation. In the vicinity of resonance, the power losses are low and nearly identical for both modes, ranging from about 8×10^{-5}/mm to 8.3×10^{-4}/mm. Since these losses are negligible, the coupling length L_c can be estimated (with less than 2 % error) by [2]

$$L_c = \frac{\pi}{\delta}. \tag{12}$$

The grating period $\Lambda = 14.0387\,\mu$m, corresponding to $\delta_{\min}/k \approx 6.5 \times 10^{-4}$ produces a coupling length of about 11.5 mm or 7,700 grating periods for a grating depth of $0.01\,\mu$m. This long coupling length occurs because of the very weak grating. Stronger gratings produce much shorter coupling lengths.[2] The grating period at the point when δ is a minimum differs only slightly from the grating period when $\alpha_A = \alpha_B$.

The propagation characteristics described in Fig. 4 illustrate the standard behavior for typical GADC devices which exchange power between bound modes. A key point for the GADC is that the modal losses are negligible for the typical GADC so that the coupling efficiency approaches 100 percent, and the coupling length is given by Eq. (12).

IV. Leaky Mode Grating-Assisted Directional Couplers

Consider now the structure of the semiconductor/glass LM-GADC, as shown in Figs. 1 and 2, with parameters given in Table II. In the leaky mode coupler, sub-waveguide S refers to the semiconductor waveguide while sub-waveguide G refers to the glass waveguide. We assume that there are no material losses in the layers, and the vacuum wavelength is 1.55 μm. At grating periods far below resonance, the two modes A and B have negligible interaction. The field of mode A is confined primarily to the semiconductor sub-waveguide while the field of mode B is confined to the glass sub-waveguide. The effective index of mode A is approximately 3.2 while the effective index of mode B is about 1.48. Since the refractive index of the semiconductor material is much larger than that of the glass, mode B is always lossy with power leaking to the semiconductor substrate. This is illustrated in Fig. 3 where the "dispersion curve" for mode B always lies in the substrate fast wave region. (For the GADC with layer parameters given in Table I, the superstrate and substrate fast wave regions are almost identical and neither mode's dispersion curve lies in a fast wave region.)

The complex propagation constants for the two modes of the LM-GADC are shown in Fig. 5 for a grating depth of 0.287 μm. The space harmonic $n = 0$ of mode A interacts with the $n = 1$ space harmonic of mode B. This interaction point corresponds to the intersection point $I_{0,1}$ of Fig. 3. The propagation constants of the two modes split, Fig. 5(b), as

they approach resonance while the attenuation curves (Fig. 5(b)) cross. The minimum value of $\delta_{min}/k \approx 5 \times 10^{-4}$ occurs at the grating period $\Lambda = 0.86569\,\mu$m. Using Eq. (12), assuming the minimum value of δ, the calculated coupling length is $L_c \approx 1.5$ mm, which is approximately 1,790 grating periods. However, this estimated coupling length is too large because the modal attenuation affects the true coupling length. (The optimized coupling length, discussed later, is about 1.25 mm, or about 1,440 grating periods.)

As can be seen from Fig. 5(a), the curves representing the attenuation constants cross at $\Lambda \approx 0.86525\,\mu$m, somewhat below the resonant point when δ is a minimum ($\Lambda \approx 0.86569\,\mu$m). Near resonance, the attenuation of mode B has a maximum, while the attenuation of mode A is a minimum. These two features are usually exhibited in a resonant system and indicates that a stop band occurs for mode B while mode A is in a passband.

The two key layer thicknesses affecting the coupling length and the amount of power coupled from the region in the vicinity of sub-waveguide S to the region in the vicinity of sub-waveguide G, are (1) grating depth and (2) the thickness of the spacer layer (Table II). In the present example, the tooth height is $0.287\,\mu$m and the grating period is approximately $0.86\,\mu$m.

Because of the presence of the grating layer, the fields of the LM-GADC and the GADC structures are expanded in an infinite number of space harmonics. While the complete field distributions consist of the summation of all space harmonics, there are only a few space harmonics with significant amplitudes. Away from resonance, only one space harmonic is dominant, whereas at least two space harmonics have significant amplitudes at the resonant condition. For mode A, the n = 0 and -1 space harmonics are dominant, while other space harmonics are negligible. For mode B, the n = 0 and 1 space harmonics are dominant, while the others are negligible.

The complete field pattern can be obtained by the summation of all spatial harmonics. Figure 6 shows the total field distributions of mode A and mode B, where mode A represents the "in-phase" (no zero-crossings of the electric field distribution between the waveguides) solution, and mode B displays the "out-of-phase" (a single zero-crossing of the electric field distribution between the waveguides) solution. (The imaginary part of the fields are also shown in the figure.) Note that both field distributions have almost identical intensities in both sub-waveguides. It is the inclusion of the space harmonics that produces the "in-phase" and "out-of-phase" solutions for the two modes. The addition or subtraction of these two solutions puts the tandem waveguide power in either sub-waveguide S or sub-waveguide G. In other words, a linear combination of the two modes can produce a field distribution with most of the light in one of the waveguides. The fine structure on the field patterns in Fig. 6 indicates the excitation of higher-order space harmonics.

The propagation characteristics shown in Fig. 5 are plotted as a function of the grating period. Although this is not a true "$\omega-\beta$" plot it illustrates modal characteristics as a function of grating period. A "classic dispersion" curve is shown in Fig. 7. Again, the figure represents the characteristics in the neighborhood of the intersection point $I_{0,1}$. The pairs of dots correspond to specific values of the grating period. The dots and corresponding field distributions are given for three different grating periods, (1) a Λ value below resonance, (2) a Λ value at resonance and (3) a Λ value above resonance. Below resonance, mode

A is confined to the semiconductor sub-waveguide and mode B is confined to the glass sub-waveguide. Above resonance, mode A has most of its power confined to the glass sub-guide and mode B is confined to the semiconductor sub-guide.

The two modes switch their "mode profile signatures" as they progress through resonance. It is interesting to note that the modal group velocity is $v_g = c/(d\beta/dk)$ for the propagating mode. (All space harmonics associated with the mode propagate with the same group velocity v_g. This implies the mode maintains a given shape as it propagates.) The definition of the group velocity implies $d\beta/dk$ behaves as an effective group index, n_g. The value of the effective group index is a measure of where the optical intensities are confined. For example, the effective group index of a mode confined to the glass waveguide is approximately equal to the refractive index of the glass. (Because $n_g > 1$, the slope of the curves in Fig. 7 can never be greater than 1.) Below resonance, the effective group index of mode A, n_{gA}, is approximately equal to the effective group index of mode B, n_{gB}, above resonance. Likewise, n_{gB}, below resonance is approximately equal to n_{gA} above resonance. In the former case, a majority of the optical power is confined to the semiconductor, whereas, in the latter case, a majority of the optical power is confined to the glass guide. As the two modes progress through resonance, they reach the point when $n_{gA} = n_{gB}$. This condition implies that each mode has very similar optical distributions. Specifically, the "in-phase" and "out-of-phase" modes have nearly identical intensity patterns.

V. The Coupling Mechanism

Excitation of the coupler from an external source such as a connecting waveguide will generate all of the modes of the LM-GADC. To minimize scattering at their interface, the fields of the two waveguides (exciting and coupler waveguides) must have similar shapes. A "smooth transition" can be obtained with an exciting guide that is almost identical to the LM-GADC waveguide. In the present case, the exciting waveguide will be assumed to be identical to the coupler waveguide, except the input waveguide will not have a grating at the semiconductor/glass interface (see Fig. 1). The input waveguide has two trapped modes: one mode's fields are predominantly confined to the semiconductor sub-waveguide, while the second mode will have fields predominantly confined to the glass sub-waveguide. When the exciting waveguide contains an incident field composed of only the semiconductor mode, the fields in the semiconductor portion match the fields of each of the two coupler modes. Near resonance, both coupler modes will be excited with almost equal amplitudes, and the field in the glass sub-waveguide is negligible.

The two Floquet-Bloch modes of the LM-GADC are in general nonorthogonal. As they propagate in the z direction, there may be an exchange of power from one mode to the other. (This power exchange between modes is not our present concern.) The primary focus here is to understand how to transfer or "couple" power between the two sub-waveguides. In particular, we discuss how to transform an initial power distribution with power concentrated in the semiconductor sub-waveguide, say at $z = 0$, to a transverse power distribution with power concentrated in the glass sub-waveguide, at the distant point $z = L_g$. Physically, the LM-GADC will be excited from the semiconductor/glass waveguide section using the semiconductor mode that is incident from the $z < 0$ region. The excitation at $z = 0$ dictates how the power is partitioned between the two Bloch modes.

At resonance, the field shapes of the Bloch modes have special and interesting characteristics. (Neither Bloch mode can be normalized in the transverse direction, $-\infty < x < \infty$, using their intensity distributions. However, we have normalized their intensity patterns in the vicinity of the tandem waveguide using finite limits on x, including layers 2 through 15 of Table II.) By choosing a particular phase of one mode relative to the other, both Bloch modes have peak values (real parts) in the sub-waveguide S, however, the fields in the sub-waveguide G are out of phase.

To appreciate the special shapes of the complex LM-GADC modes at resonance, we explore how a combination of the two modes allows an excellent match to an input exciting field. The general solution to the fields in the coupler must be written as a linear combination of the two Floquet-Bloch modes as

$$E_y(x,z) = a_A\, f_A(x,z)\, e^{-\gamma_A z} + a_B\, f_B(x,z)\, e^{-\gamma_B z}, \tag{13}$$

where a_A and a_B are the expansion coefficients that measure the partition of the power into the modes. For the present discussion, assume the coupler is excited with all the power in the semiconductor sub-waveguide. At the input $z = 0$, the field in the coupler is obtained by summing the two modes of Fig. 6, implying $a_A = a_B = 1/2$. As the two modes progress along the z direction, the continuously evolving field shape amounts to a redistribution of power in the sub-waveguides of the composite waveguide.

We estimate the powers P_A and P_B in sub-waveguides S and G respectively, as [2]

$$P_S = -\frac{1}{2}\mathrm{Re}\int_0^{\infty} E_y H_x^*\, dx,$$
$$P_G = -\frac{1}{2}\mathrm{Re}\int_{-\infty}^{0} E_y H_x^*\, dx.$$

For the structure whose dispersion characteristics are shown in Fig. 5, the percentage of the total input power coupled to the glass waveguide, as a function of grating length L_g, is shown in Fig. 8. At the excitation point, the total waveguide power is concentrated in the semiconductor side. The power is transferred to the glass as the LM-GADC modes propagate.

Figure 8 also shows the coupled power versus grating length with various grating periods of the LM-GADC structure of Fig. 1. The curves indicate that the maximum coupling drops as the coupler is detuned from resonance. At resonance, we obtain the maximum coupled power and the optimum coupling length. Off resonance, both the coupled power and the optimum coupling length are reduced. As shown in Fig. 8, the maximum coupled power is greater than 40 % with a coupling length of 1.25 mm, and the optimum grating period is $0.8657\,\mu$m.

We now determine the coupling characteristics from the raw dispersion data of Fig. 7. Due to the "symmetric" and "asymmetric" shapes of the two fields illustrated in Fig. 6, it is convenient to write the fields in terms of two functions $s(x)$ and $g(x)$. The function $s(x)$ represents the field distribution in the semiconductor sub-waveguide while $g(x)$ represents

the field in the glass sub-waveguide. In addition, the two functions satisfy:

$$s(x) \approx 0 \quad \text{for} \quad x \in \text{Glass sub-waveguide},$$
$$g(x) \approx 0 \quad \text{for} \quad x \in \text{Semiconductor sub-waveguide}.$$

It is interesting to note that the function $s(x)$ is approximately equivalent to the field distribution of the semiconductor mode in the absence of a grating layer. Similarly, the function $g(x)$ is approximately equivalent to the field distribution of the glass mode in the absence of the grating layer. Thus, when the LM-GADC is excited with the "semiconductor mode", the excitation field shape is $s(x)$. On the other hand, when the LM-GADC is excited with a "glass mode", the excitation field shape is $g(x)$.

The overall field distribution as given by Eq. (1) across the layers can be written as

$$f(x,z) = f^{(i)}(x,z) \quad \text{for} \quad x \in i\text{th layer}.$$

Due to the nature of the field shapes as shown in Fig. 6, the Floquet-Bloch modes can be approximated with the two dominant space harmonics of modes A and B. These dominant space harmonics are characterized by the two functions $s(x)$ and $g(x)$,

$$f_A(x,z) = s(x) + g(x)e^{jKz},$$
$$f_B(x,z) = s(x)e^{-jKz} - g(x).$$

Using the approximate expressions for the modes, the total field becomes (putting $a_A = a_B = 1/2$)

$$E_y(x,z) = \frac{1}{2}[s(x) + g(x)e^{jKz}]\, e^{-\gamma_A z} + \frac{1}{2}[s(x)e^{-jKz} - g(x)]\, e^{-\gamma_B z}.$$

At an arbitrary position, z, the total field becomes

$$E_y(x,z) = \frac{1}{2}\left\{[s(x) + g(x)e^{jKz}] + [s(x)e^{-jKz} - g(x)]\, e^{-(\gamma_B - \gamma_A)z}\right\} e^{-\gamma_A z}.$$

As seen from Fig. 5, the attenuation coefficients of the two modes near resonance have approximately equal values ($\alpha_A \approx \alpha_B$), so that the term $\alpha_B - \alpha_A$ can be dropped, so that the exponent $\gamma_B - \gamma_A = \alpha_B - \alpha_A + j(\beta_B - \beta_A) \approx j(\delta - K)$. The resulting field simplifies to

$$E_y(x,z) = e^{-j\frac{1}{2}\delta z}\left[s(x)\cos(\frac{1}{2}\delta z) + jg(x)e^{jKz}\sin(\frac{1}{2}\delta z)\right] e^{-\gamma_A z}. \tag{17}$$

The first term in the brackets characterizes the field in the semiconductor guide while the second term characterizes the field in glass. To find the optimum coupling length, where the power in the glass guide is maximized, the magnitude of the second term must be maximized relative to z, and the optimum z value will represent the best coupling length. In the optimization process, the phase term $\exp[j(K - \beta_a)z]$ is dropped because the envelope amplitude, characterized by $\sin(\delta z/2)\exp(-\alpha_A z)$, is to be maximized. After simplification, the optimum coupling length L_c is found to be a solution to the transcendental equation

$$\tan\frac{\delta}{2}L_c = \frac{\delta}{2\alpha}. \tag{18}$$

(Because the attenuation coefficients are approximately equal, the term α_A has been replaced by α.) Although the results obtained for the optimum coupling length assumes approximately equal values of attenuation for both modes, a similar result can be obtained when modal attenuations are different. In the limiting case of $\alpha \to 0$, Eq. (18) reduces to Eq. (12).

To determine the coupling length for optimum power transfer for the structure described in Table II, the value of the deviation coefficient $\delta = \delta_{\min} = (5 \times 10^{-4})k$ and $\alpha \approx (7.5 \times 10^{-5})k$ are substituted into Eq. (18). These optimum values produce a coupling length of $L_c \approx 1.25mm$ which agrees with the value obtained from the numerical computations for the coupling efficiency, shown in Fig. 8.

VI. Optimization

The coupling depends on the combination of the difference between β_0^A and β_1^B and the attenuation coefficients of the modes. In many cases modal attenuation is a dominant factor resulting in low power transfer. When one mode attenuates much faster than the second, it is difficult to achieve high percentages of power transfer. A major result of this analysis is that the attenuation of the Bloch modes plays a significant role in determining the optimum coupling length in grating couplers.

The field distributions of the two Floquet-Bloch modes evolve as the $\omega - \beta$ plot progresses through resonance. As the modes exchange their "signatures", there is a single point where both have the same group velocity and the deviation wavenumber δ is minimized. This implies that they have almost equal intensity shapes. When this condition occurs, the usual "in-phase" and "out-of-phase" fields allow for a linear combination of the modes to produce a distribution of power which is concentrated in one waveguide or the other. If the modes are combined (say added) with equal amplitudes, the resulting field places the power in the semiconductor sub-waveguide. Likewise if the modes are subtracted, the power is placed in the glass sub-waveguide. Furthermore, when one mode vanishes over a distance smaller than π/δ, only one mode remains and field shape in the composite waveguide is invariant with z. Therefore, to find the maximum coupling, the attenuation characteristics of the two modes must be evaluated.

The key parameter that affects modal attenuation is the coupling strength. (Both the grating depth, period and grating duty cycle affect the coupling strength. A 50 % duty cycle is used in all of our calculations.) Figure 9 shows the normalized attenuation coefficient as a function of grating depth for modes A and B. The grating period is fixed at $0.8670\,\mu$m, which is well below the resonant condition. In addition, the thickness of layer 6 (see Table II), is $0.3175\,\mu$m. It should be noted that other values of the grating period and spacer layer thickness produce a differently shaped curve, but all resulting curves are similar in that their maximum and minimum values of α lie in ranges similar to those shown in Fig. 9. Namely, mode A has minimum α values at grating depths near 0 and $0.3\,\mu$m. Attenuation of mode B is rather insensitive to grating depth.

Grating depths that produce the best coupling efficiency are in those ranges where α_A is very close to α_B. In addition, these ranges correspond to the smallest values of attenuation. These best ranges occur at grating depths near 0 and $0.3\,\mu$m. At grating depths near 0,

the coupling strength is very small which produces very small $\delta_{\min}$ values. These small $\delta_{\min}$ values extrapolate to relatively long coupling lengths L_c that are typically impractical. When the grating depth is increased, the difference of the two attenuations α_A and α_B increases. Although the LM-GADC structure changes coupling strength with an increased tooth height, the low values of either $1/\alpha_A$ or $1/\alpha_B$, the length when the mode amplitude drops to 1/e of its initial value, are smaller than computed values of $1/\delta_{\min}$ where the best coupling length occurs. Thus, the mode attenuates before a 180° relative phase change occurs. For tooth heights near zero, the coupling efficiency is generally below 10 percent while for grating depths near $0.3\,\mu$m, the coupling efficiency is about 40 percent.

The coupled power to the glass region as shown in Fig. 8 reaches a peak value and then drops back to near zero. This classic oscillation (with auxiliary attenuation due to leakage of power) occurs because power shifts back and forth between the two sub-waveguides. The power in the semiconductor sub-waveguide oscillates out of phase relative to the power in the glass sub-waveguide. At the optimum coupling length when the power in the glass peaks, the power in the semiconductor waveguide is at a minimum.

Figure 10 shows the coupled power as a function of tooth height, assuming the parameters given in Table II. In fact the optimum value of approximately 40 % or about 4 dB, occurs at a grating depth of $0.287\,\mu$m. The optimum coupling length is $L_c \approx 1.25$mm. Even though the coupling length L_c increases for grating depths above $0.287\,\mu$m, the coupling efficiency drops.

When the grating period Λ, or the wavelength λ is changed, the optimum coupling is reduced. For example, in Fig. 8, the grating period $\Lambda = 0.8657\,\mu$m requires the coupler to have a length of $L_g = 1.25\,$mm. If the actual length is different from 1.25 mm, the coupling efficiency will be decreased.

A characteristic of the LM-GADC is its frequency selectivity or its narrow-banded property. Using the results of Fig. 8, the coupling efficiency for the 1.25 mm length LM-GADC as a function wavelength deviation $\delta\lambda$ about $\lambda = 1.55\,\mu$m is shown in Fig. 11. We find the FWHP of the coupling bandwidth is about 9 $\mathring{\text{A}}$.

VII Conclusion

Floquet-Bloch analysis has been been applied to the study of LM-GADCs that are fabricated with two very different materials such as semiconductor materials (refractive index of approximately 3.2) and glass (refractive index of about 1.48). The complex propagation constants of the two lowest-order modes of the tandem waveguide system are determined versus various parameters such as grating period and grating depth. Assuming the semiconductor and glass waveguide dimensions and refractive indices are those given in Table II, the optimum grating depth is $0.28\,\mu$m. The resulting coupling efficiency is about 40 percent, or about 4 dB, and the optimum coupling length is 1.25 mm. The grating period at the optimum is about $0.86\,\mu$m.

The coupling efficiency obtained by this method is applicable to the two dimensional model where the slab has infinite extension in the lateral direction. Generally, slab models are applicable to similar three dimensional structures when the widths of the modes in the

lateral (y-axis) dimension are large compared to the widths in the transverse (x-direction) dimension.

The simple LM-GADC is not an efficient coupler compared to the GADC. While the GADC of Table I can transfer almost 100 percent of its power from one region (first sub-waveguide) to a second region (second sub-waveguide), the LM-GADC of Table II can transfer only about half of its input power from one guide to a second guide. The major reason for this difference is due to the fact that the LM-GADC has more radiation loss and the corresponding modal attenuation plays a dominant role in determining the optimum transfer length. By incorporating multilayer reflective stacks in the substrate, we expect the coupling efficiency can be increased to 70%. In the present examples, the modal attenuation of the LM-GADC of Table II is about one order of magnitude greater than the modal attenuation of the GADC of Table I. The LM-GADC losses are due mainly to power leaking to the substrate.

Finally, Floquet-Bloch modes exchange "signatures" as they progress through resonance. The classical coupling length (when losses are negligible such as for the GADC), is determined from the minimum longitudinal propagation constant separation, δ_{min}, using Eq. (12). When losses become significant (such as with the LM-GADC), the coupling length must be determined from Eq. (18).

References

[1] D. Marcuse, "Radiation loss of grating-assisted directional coupler," *IEEE J. Quantum Electron.*, vol. QE-26, no. 4, pp. 675–684, Apr. 1990.

[2] N. H. Sun, J. K. Butler, G. A. Evans, L. Pang, and P. Congdon, "Analysis of grating-assisted directional couplers using floquet bloch theory," *IEEE J. Lightwave Tech.*, vol. 15, no. 12, pp. 2301–2315, Dec. 1997.

[3] D. Marcuse, "Directional couplers made of nonidentical asymmetric slabs. part i: Synchronous couplers," *IEEE J. Lightwave Tech.*, vol. LT-5, no. 1, pp. 113–118, Jan. 1987.

[4] D. Marcuse, *Theory of Dielectric Oprical Waveguides*, Academic Press, San Diego, 2nd ed. edition, 1991.

[5] W. P. Huang and H. A. Haus, "Power exchange in grating-assisted couplers," *IEEE J. Lightwave Tech.*, vol. LT-7, no. 6, pp. 920–924, June 1989.

[6] H. A. Haus, W. P. Huang, S. Kawakami, and N. A. Whitaker, "Coupled-mode theory of optical waveguides," *IEEE J. Lightwave Tech.*, vol. LT-5, no. 1, pp. 16–23, Jan. 1987.

[7] W. P. Huang, B. E. Little, and S. K. Chaudhuri, "A new approach to grating-assisted couplers," *IEEE J. Lightwave Tech.*, vol. LT-9, no. 6, pp. 721–727, June 1991.

[8] W. P. Huang and J. W. Y. Lit, "Nonorthogonal coupled-mode theory of grating-assisted codirectional couplers," *IEEE J. Lightwave Tech.*, vol. LT-9, no. 7, pp. 845–852, July 1991.

[9] W. P. Huang, J. Hong, and Z. M. Mao, "Improved coupled-mode formulation based on composite mode for parallel grating-assisted co-directional couplers," *IEEE J. Quantum Electron.*, vol. QE-29, no. 11, pp. 2805–2812, Nov. 1993.

[10] W. P. Huang, "Coupled-mode theory for optical waveguides: An overview," *J. Opt. Soc. Am. A*, vol. 11, no. 3, pp. 963–983, Mar. 1994.

[11] B. E. Little, W. P. Huang, and S. K. Chaudhuri, "A multiple-scale analysis of grating-assisted couplers," *IEEE J. Lightwave Tech.*, vol. LT-9, no. 10, pp. 1254–1263, Oct. 1991.

[12] B. E. Little and H. A. Haus, "A variational coupled-mode theory for periodic waveguides," *IEEE J. Quantum Electron.*, vol. QE-31, no. 12, pp. 2258–2264, Dec. 1995.

[13] B. E. Little, "A variational coupled-mode theory including radiation loss for grating assisted couplers," *IEEE J. Lightwave Tech.*, vol. LT-14, no. 2, pp. 188–195, Feb. 1996.

[14] V. M. N. Passaro and M. N. Aremise, "Analysis of radiation loss in grating-assisted co-directional couplers," *IEEE J. Quantum Electron.*, vol. QE-31, no. 9, pp. 1691–1697, Sept. 1995.

[15] W. P. Huang and H. Hong, "A transfer matrix approach based on local normal modes for coupled waveguides with periodic perturbations," *IEEE J. Lightwave Tech.*, vol. LT-10, no. 10, pp. 1367–1375, Oct. 1992.

[16] S. T. Peng, T. Tamir, and H. L. Bertoni, "Theory of periodic dielectric waveguides," *IEEE Trans. Microwave Theory Tech.*, vol. MTT-23, no. 1, pp. 123–133, Jan. 1975.

[17] K. C. Chang, V. Shah, and T. Tamir, "Scattering and guiding of waves by dielectric gratings with arbitrary profiles," *J. Opt. Soc. Am.*, vol. 70, pp. 804–813, July 1980.

[18] G. Hadjicostas, J. K. Butler, G. A. Evans, N. W. Carlson, and R. Amantea, "A numerical investigation of wave interactions in dielectric waveguides with periodic surface corrugations," *IEEE J. Quantum Electron.*, vol. QE-26, no. 5, pp. 893–902, May 1990.

[19] J. K. Butler, W. E. Ferguson, G. A. Evans, P. J. Stabile, and A. Rosen, "A boundary element technique applied to the analysis of waveguides with periodic surface corrugations," *IEEE J. Quantum Electron.*, vol. QE-28, no. 7, pp. 1701–1709, July 1992.

[20] R. L. Burden and J. D. Faires, *Numerical Analysis*, PWS-KENT, Boston, fourth edition, 1984.

Layer	Thickness(μm)	Refractive Index
1 Superstrate	∞	3.180
2 Sub-waveguide B	0.200	3.282
3 Cladding	1.450	3.180
4 Grating	0.010	3.180/3.282
5 Step	0.450	3.282
6 Sub-waveguide A	0.257	3.450
7 Substrate	∞	3.180

Table I: The parameters of grating assisted directional couplers using two similar sub-waveguides.[1] The free-space wavelength is $\lambda_0 = 1.5\,\mu$m. "Sub-waveguide A" includes layers 5 and 6 while "sub-waveguide B" includes layer 2.

Layer	Thickness(μm)	Refractive Index
1 Glass Cladding	∞	1.448
2 Glass Cladding	3.0000	1.448
3 Glass Waveguide	5.0000	1.458
4 Glass Cladding	1.0000	1.448
5 Grating Layer	0.2870	3.165/1.448
6 Spacer	0.3175	3.165
7 Confining Layer	0.1200	3.386
8 Quantum Well	0.0090	3.532
9 Barrier	0.0100	3.386
10 Quantum Well	0.0090	3.532
11 Barrier	0.0100	3.386
12 Quantum Well	0.0090	3.532
13 Barrier	0.0100	3.386
14 Quantum Well	0.0090	3.532
15 Confining Layer	0.1200	3.386
16 Substrate Cladding	1.0000	3.165
17 Substrate	∞	3.165

Table II: The parameters of grating assisted directional couplers using two different sub-waveguides. Sub-waveguide S consists of layers 7 through 15, while sub-waveguide G consists of layer 3. The free-space wavelength is $\lambda_0 = 1.55\,\mu$m.

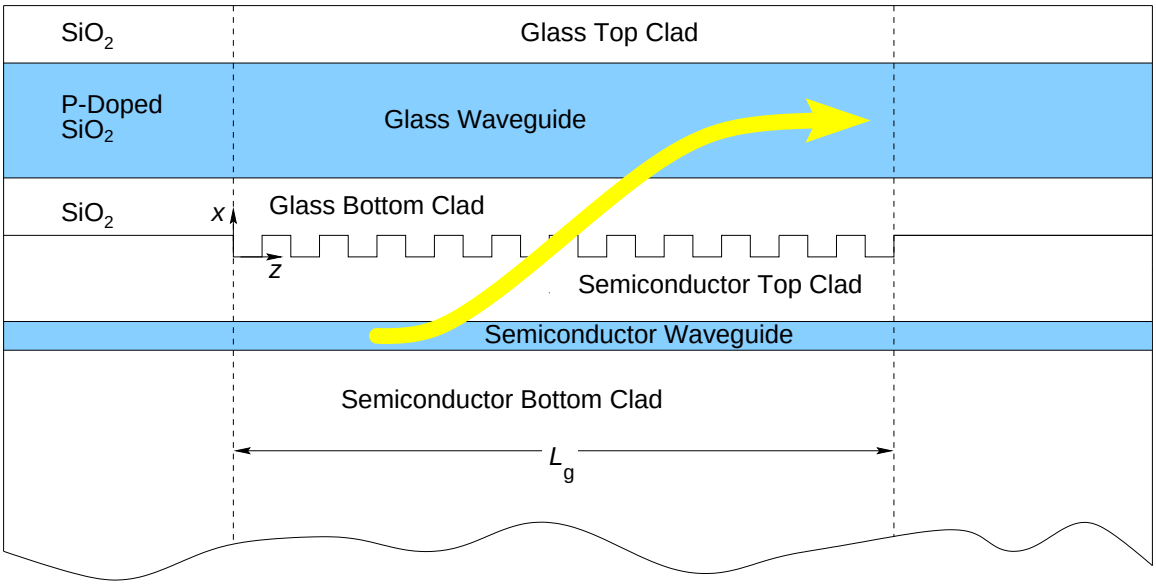

Figure 1: The cross section of an integrated semiconductor-glass waveguide. The grating is etched into the semiconductor cladding region and the glass waveguide is deposited over the grating. The grating assists in coupling light from the semiconductor sub-waveguide to the glass sub-waveguide and vice versa.

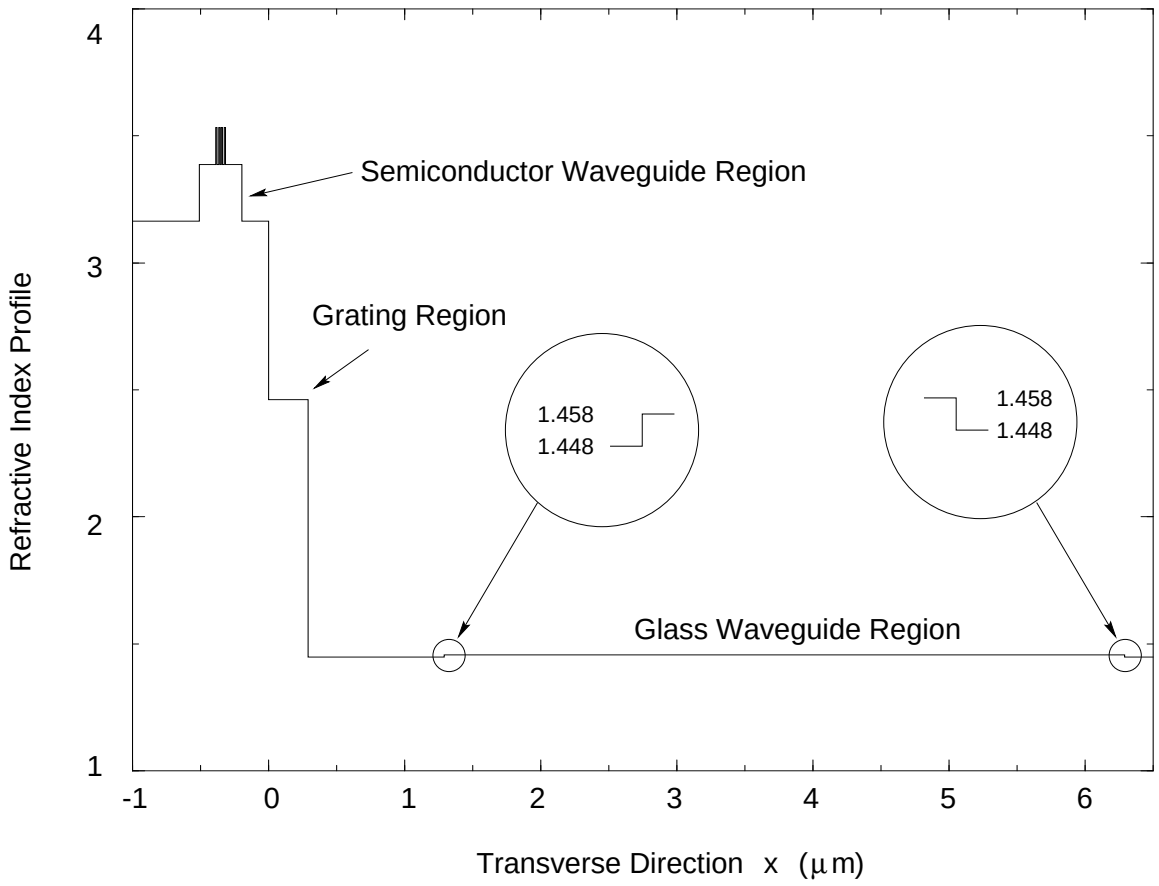

Figure 2: The refractive index profile of the semiconductor-glass waveguide configuration. The bottom of the grating is the orgin.

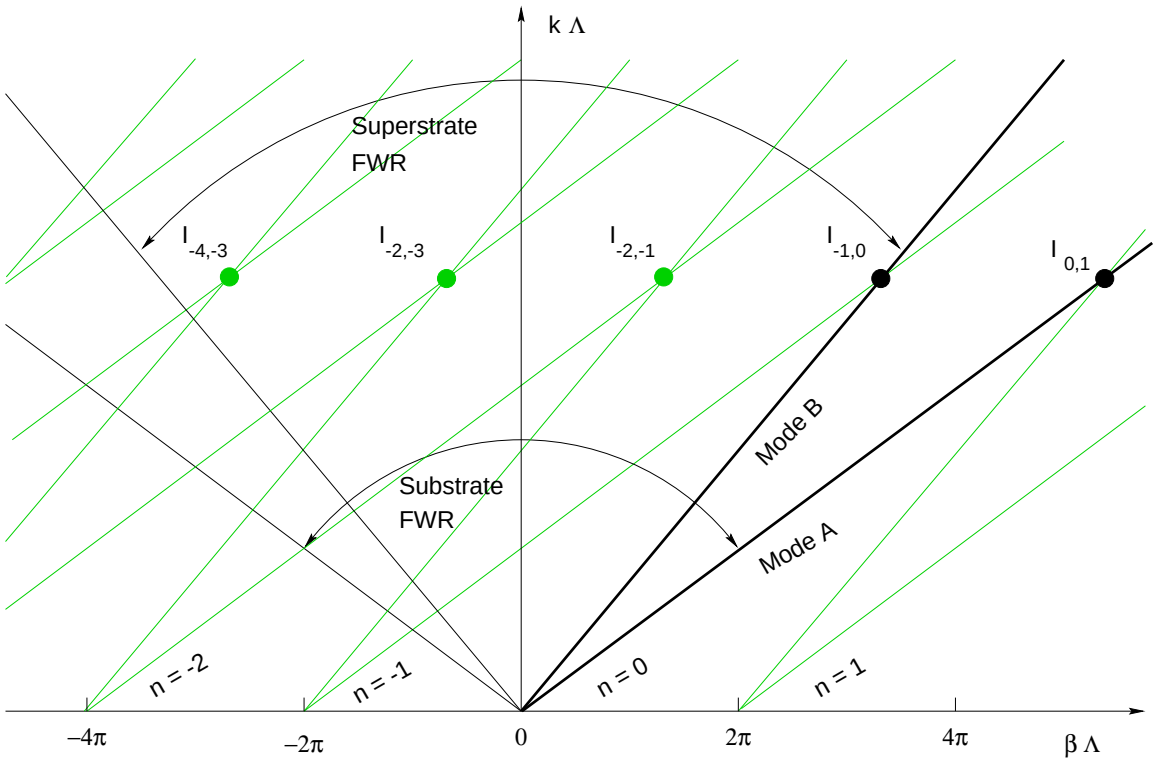

Figure 3: The kinematic properties of the co-directional coupling of two Floquet-Bloch modes. Mode A represents the mode of the "semiconductor waveguide", while Mode B is the mode of the "glass waveguide."

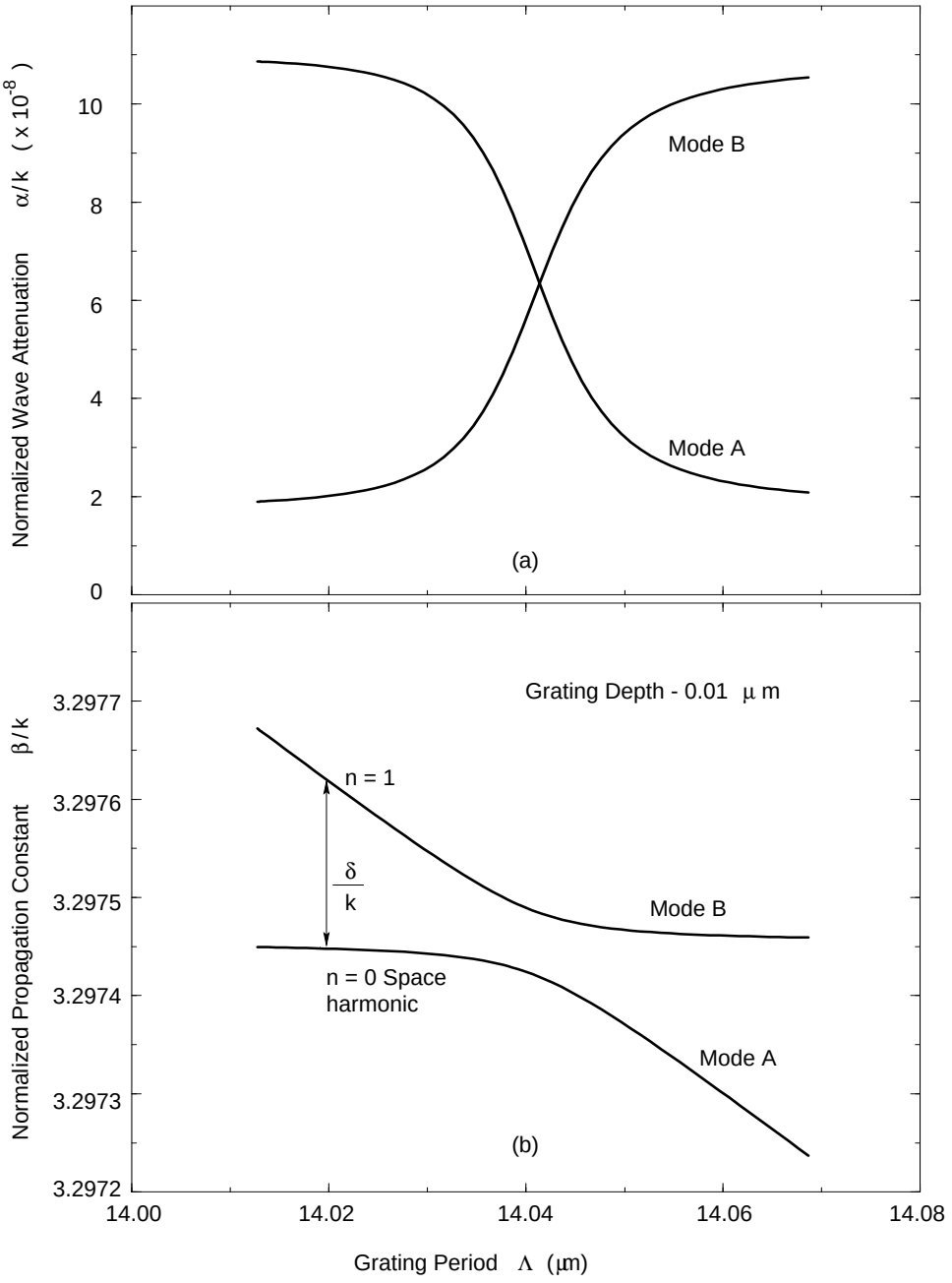

Figure 4: The complex propagation constant of the two Floquet Bloch modes, mode A and mode B, for a GADC. The grating depth is $0.01\,\mu$m. (a) The modal $x =$attenuation coefficients which cross, and (b) the propagation constants of the two space harmonics which split at resonance. The minimum separation , $\delta_{\min}/k$ of 6.5×10^{-5}, occurs at $\Lambda = 14.041\,\mu$m.

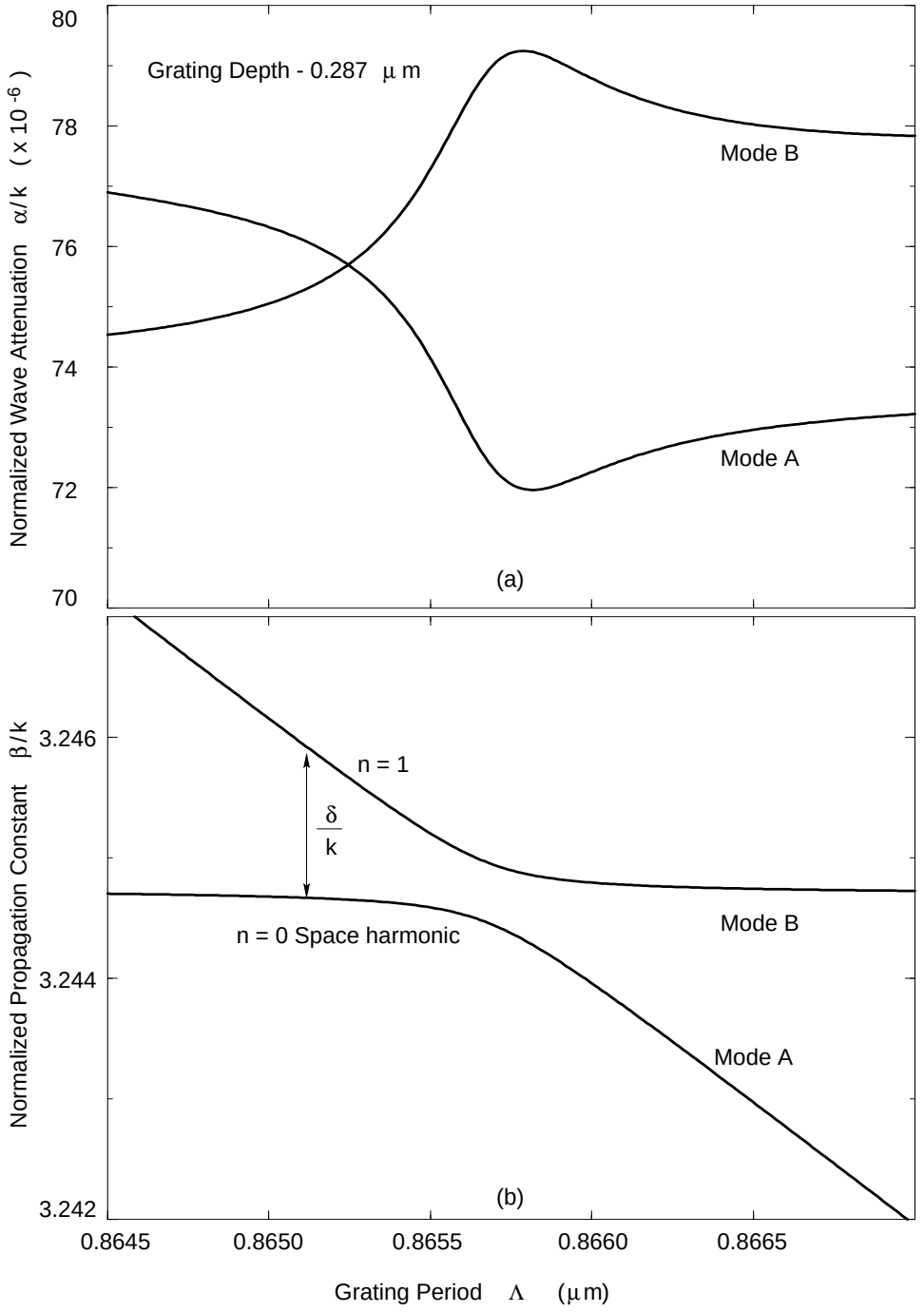

Figure 5: The complex propagation constant of the two Floquet Bloch modes, Mode A and Mode B, for a LM-GADC representing the semiconductor-glass waveguide configuration. The grating depth is $0.287\,\mu$m. (a) The attenuation constant for the two modes, and (b) the propagation constants of the two space harmonics which split at resonance. The mimimum separation, $\delta_{\min}/k$ of 5×10^{-4}, occurs at $\Lambda = 0.86569\,\mu$m.

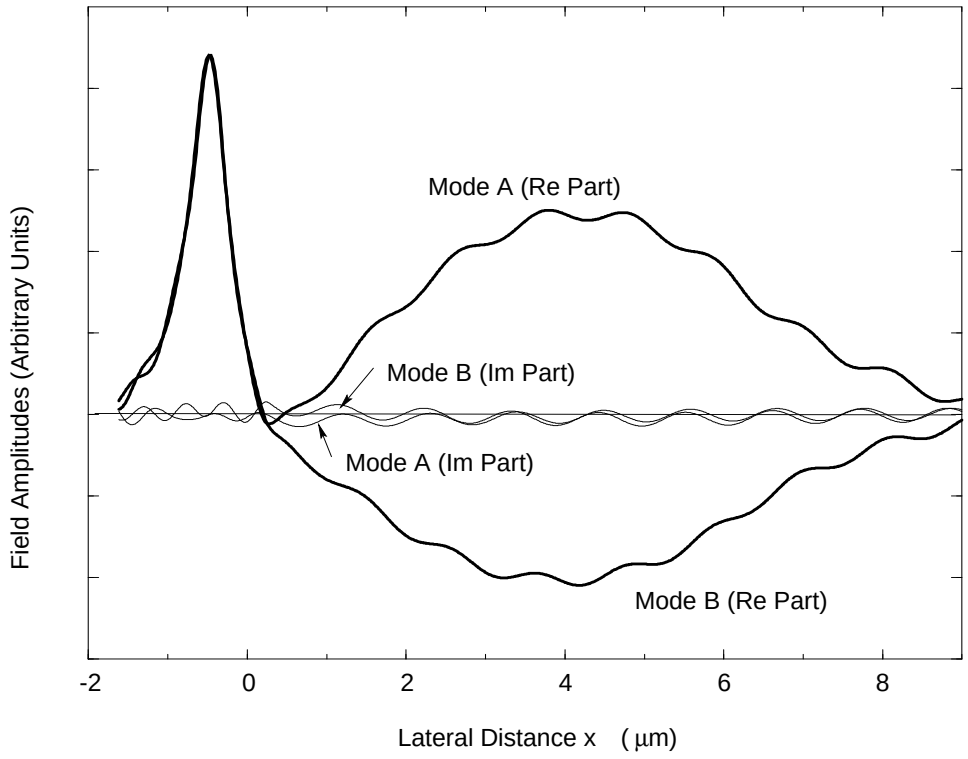

Figure 6: The optical field distribution at resonance. Mode A represents the "in-phase" mode while B is the "out-of-phase" mode. The term Re is for the real part of the field and Im stands for the imaginary part.

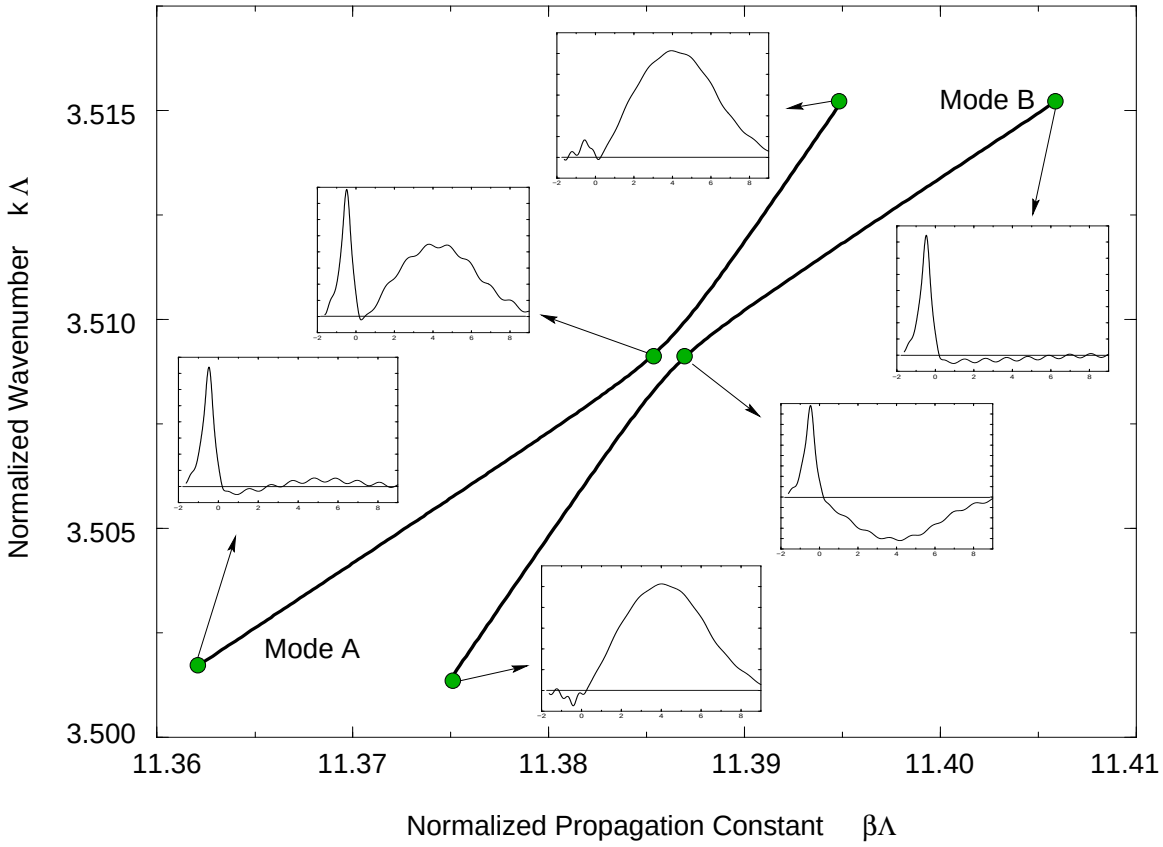

Figure 7: The "$\omega - \beta$" diagram at the intersection $I_{0,1}$. The field inserts in the figure are the real parts of the fields. The corresponding imaginary parts, not shown, are relatively small.

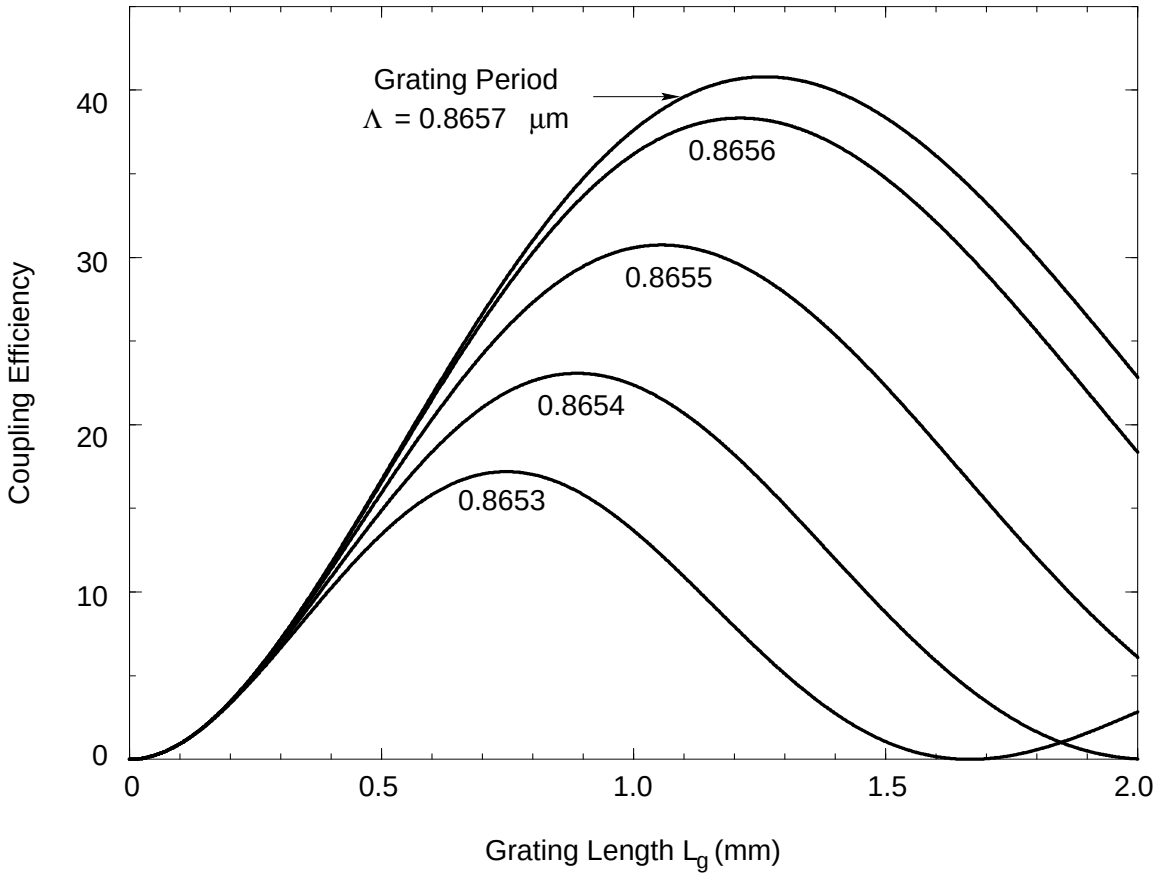

Figure 8: The coupling efficiency as a function of propagation distance.

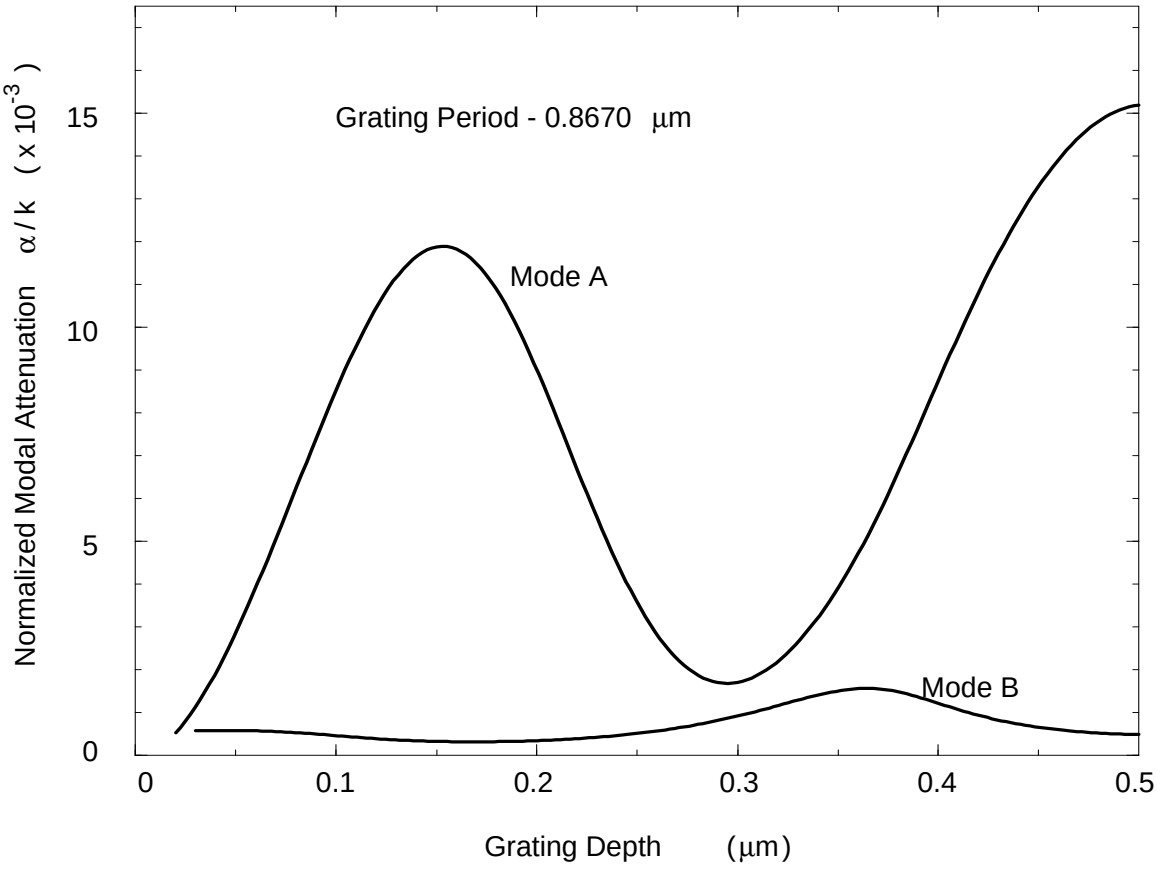

Figure 9: The normalized modal attenuation for the LM-GADC as a function of tooth height. The grating period is fixed at $0.8670\,\mu m$. The grating period chosen for this calculation is not near the resonance condition.

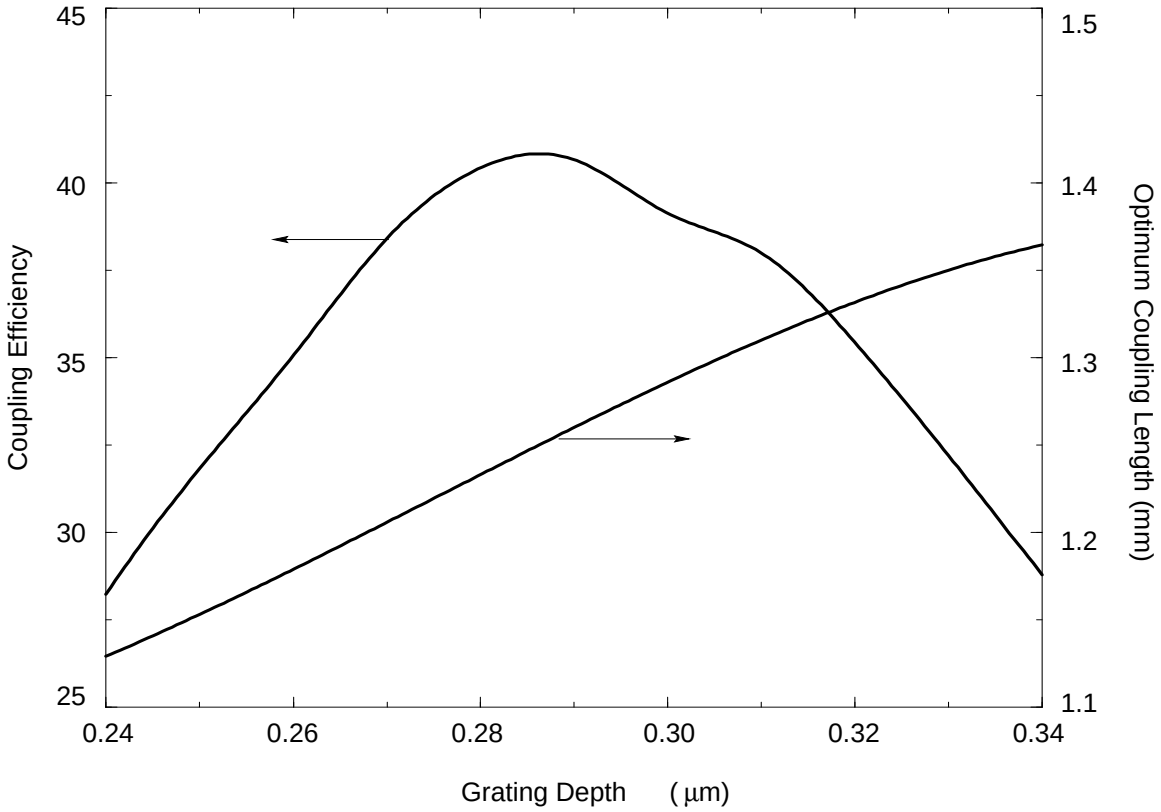

Figure 10: The effect of tooth height variations on the coupling efficiency. The waveguide parameters are given in Table II. (a) The coupling efficiency, and (b) the optimum coupling length.

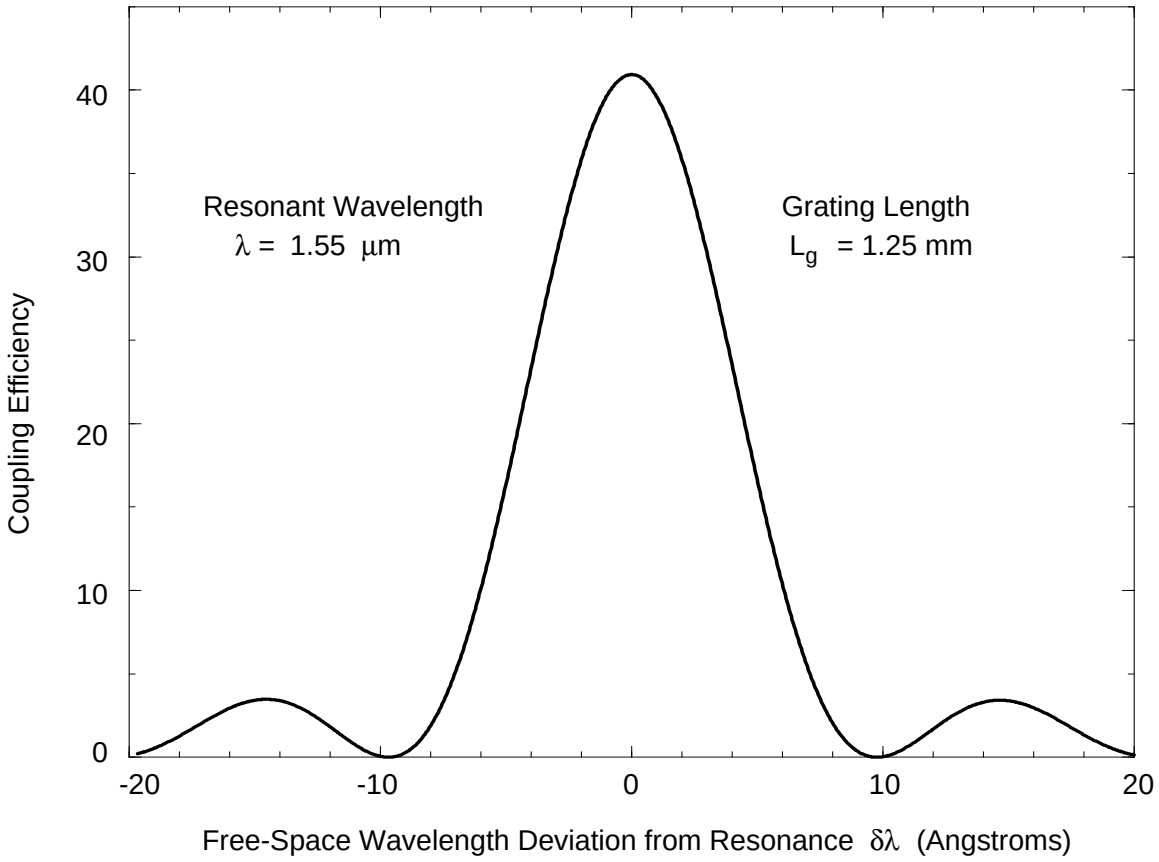

Figure 11: The coupling efficiency about the resonant wavelength, $\lambda = 1.55\,\mu$m. The resonant grating period is $\Lambda = 0.86569\,\mu$m.